

Contents lists available at ScienceDirect

Fuel

journal homepage: www.elsevier.com/locate/fuel



Full Length Article

Release, Transport, and accumulation of lithium in shale brines

Kyung Jae Lee^{a,*}, Jiahui You^a, Yongjun Gao^b, Tanguy Terlier^c

- a Department of Petroleum Engineering, University of Houston, 5000 Gulf Freeway, Houston, TX 77204, USA
- ^b Department of Earth and Atmospheric Sciences, University of Houston, 3507 Cullen Blvd, Houston, TX 77204, USA
- ^c Shared Equipment Authority, Rice University, 6100 Main St., Houston, TX 77005, USA

ARTICLE INFO

Keywords: Lithium Shale brines Energy decarbonization Critical minerals Renewable energy storage Sustainable energy system

ABSTRACT

In order to mitigate climate change, diversifying the sources of lithium supply is crucial for the decarbonization of energy sector through enhanced renewable electricity generation and electrified transportation. Shale brines have been recently found to be containing significant amount of lithium, but relevant subsurface phenomena regarding its origin, fate, and transport are unknown. Here we present a suite of geochemical experiments to elucidate the initial presence of lithium in shale rocks and its release mechanism from solid phase into fluid, and numerical modeling to estimate the resources of lithium in shale brines by addressing its fate and transport. We find that the majority of lithium is inorganically bound as an interlayer cation of clay in shale rock, while a sparingly small portion is organically bound. Hydrothermal reaction experiments for leaching lithium reveal that calcium ion in fluid has strongest impact on lithium to be released into fluid, while sodium ion has minimal impact. From the numerical modeling combined with the experimental findings, average concentration of lithium in shale brines mimicking Marcellus Shale system is estimated to be about 135 ppm under calcium ion dominancy in pore fluid, which shows excellent match with actually measured values from produced Marcellus Shale brines. This study provides the understanding of fundamental phenomena addressing release, transport, and accumulation of lithium in geologic system, and hence contributes to the enhancement of sources of lithium supply for energy decarbonization.

1. Introduction

Tackling climate change is a global mission today, which brings about the urgent need of the decarbonization of the energy sector worldwide. Significant methods to realize the energy decarbonization involve to increase the electricity generation by renewable and sustainable energy and electrification of transportation. As renewable wind—and—solar electricity generation and electrified transportation are mainly relying upon lithium (Li)—ion energy storage, global demand of Li has greatly increased during the past decade, and is expected to escalate continuously along with the market growth [1]. In line with the increasing demand, there have been recently active efforts to enhance and diversify the sources of supplying Li globally.

Land-based Li resources are unevenly distributed, where more than 98% of the total reserves are concentrated in Chile, Argentina, China, and Australia [2]. Li concentration in seawater is between 0.1 and 0.2 ppm [2], while land-based Li resources such as formation brines or solid rocks (i.e., continental brines, oilfield brines, geothermal brines, pegmatites, and certain clay deposits) present higher Li concentration of

magnitudes of from tens to thousands in formation brines and from hundreds to ten-thousands in hard rocks, respectively [3]. However, the active sources of global Li supply have been limited in pegmatites and several continental brines with shallow depth [4]. Recently petroleum source rocks (shales), which have traditionally been considered as a source of oil and gas converted from solid organic matter called kerogen in them, were found to be a potentially sustainable source of Li, given the high concentrations of Li (80–300 ppm) in water produced from the shale reservoirs and the wide distribution of the shale plays across the U. S. [5-7]. Given that total volume of produced water from Marcellus Shale is projected to be about $2,200 \times 10^9$ L for upcoming 73 years [8], produced water from Marcellus Shale is expected to provide the significant potential of Li recovery. Not only from Marcellus Shale, but from its entire shale plays, U.S. daily produces about 2.8 billion gallons of produced water [9]. In this regard, if economic production of Li from shale produced water is realized, it will be a game changer for the global Li supply. In addition, extraction of Li from natural brines including shale brines is known to be 30-50% less expensive than from hard-rock sources [10], which sheds light on the production potential of Li from

E-mail address: kjlee6@central.uh.edu (K.J. Lee).

^{*} Corresponding author.

shale brines. Li extraction methods from natural brines including shale brines involve the technologies, such as solvent extraction, precipitation, adsorption, membrane, and electrochemical method [2,11–13]. Their performances are highly affected by various factors such as Mg/Li ratio and TDS (Total Dissolved Solids) as well as Li concentration [14]. These methodologies have different strengths and weaknesses to each other, and their techno–economic feasibility is being currently tested. Although the petroleum source rocks (shale) can offer substantial opportunities for sustainable supply and renewable utilization of Li for energy storage, their successful production relies upon subsurface phenomena relating to its origin, fate, and transport, which have been unknown.

In this study, applying a suite of geochemical experiments and characterization, we elucidated the initial distribution of Li in shale rock and the mechanism of release of Li into fluid through fluid-rock interactions. These experiments were implemented using the samples of Green River Shale, which is an immature kerogen-bearing shale (with inorganic chemical compositions of 28.5 wt%-SiO2, 8.7 wt%-CaO, 6.6 wt%-Al₂O₃, 4.5 wt%-MgO, and various other components with minor fractions [15]; mineral components of dolomite, quartz, anorthite, calcite, pyrite, and illite-smectite mixed clay as obtained with X-Ray Diffraction of Supplementary Fig. 1 and Fourier Transform Infrared of Supplementary Fig. 2), to understand the mechanism of Li release from rock to pore fluid given the positive correlation between solid organic contents (content of immature organic matter) and solid Li concentrations [16-18]. Experiments with Green River Shale would help clearly understand the mechanism of Li release from rock to pore fluid during hydrothermal reaction between rock and fluid in geologic time-scale. With the reaction rate constants derived from the experimental results, we modeled the release, transport, and accumulation of Li in shale brines with a conceptual model mimicking Marcellus Shale, which is a mature kerogen-bearing shale. Results obtained by the modeling coupled experiments give insights into how the systematic estimation of Li resources in shale brines can be achieved and hence provide the quantified projection of shale brines as a sustainable source of Li supply.

2. Materials and methodology

In this section, the materials and methodologies for the whole workflow of geochemical experiments and numerical modeling to elucidate the release, transport, and accumulation of Li in shale brines are presented. The suite of geochemical experiments and characterization involve the isolation of kerogen from shale bulk rock to distinguishably understand the presence of organically and inorganically bound Li in shale rocks, quantification of ionic compositions of produced shale brines, elemental analysis of Li to quantify the Li compositions in various phases, Time-of-Flight Secondary Ion Mass Spectrometry (ToF-SIMS) analysis for understanding the initial presence of Li in solid phase without chemical extraction, hydrothermal reactions to elucidate the release mechanism of Li from solid phase into fluid through fluid--rock interactions under various solution compositions, and Brunauer-Emmett-Teller (BET) sorption analysis to quantify the specific surface area of shale rocks for the derivation of reaction rate constants. The numerical modeling method involves the conceptual three-dimensional reactive transport modeling to investigate the transport and accumulation of released Li in shale brines.

2.1. Isolation of kerogen from shale bulk rock

Kerogen was isolated from bulk rock of shale, by applying the closed–system chemical demineralization with pyrite removal and critical point drying [19]. The samples of kerogen–bearing shale were rinsed with deionized water while removing mud additives using fine–mesh sieve, and were dried in air. Then the shale samples were crushed into fine powder of $\sim 10~\mu m$ size, followed by the treatment with dichloromethane for 72 h with Soxhlet apparatus for the removal of

soluble organic matter composed of bitumen and free hydrocarbons. Then kerogen isolation was conducted through three–step chemical treatments for the removal of 1) carbonates and basic oxides with 2 L of 12 M-HCl, 2) silicates and clay with 1.2 L of 48%-HF/12 M-HCl, and 3) pyrite with 1 L acidified CrCl₂.

2.2. Ion chromatography for analyzing the produced shale brines

Ion chromatography analysis was conducted to measure the concentrations of cations including Li ion dissolved in the two samples of brines produced from Marcellus Shale, given the significant impact of cations in fluid on the dissolution and mineralization of Li through fluid–rock interactions. ThermoFisher Aquion IC was used for ion chromatography analysis of shale brines produced from Marcellus Shale, after the 500 times–diluted produced water samples were filtered with 45–60 μm filters to remove solid precipitates. The eluent was composed with 2.9 ml–methanesulfonic acid and 1 L–deionized water, and the other operational conditions were as follows: flow rate of 1.0 ml/min; injection volume of 25 μl ; isocratic mode; Dionex CS16 column; column temperature of 40 $^{\circ} C$; suppression current of 44 mA. The measurement error of ion concentration by stated methodology is known to be less than 0.05 ppm.

2.3. Li elemental analysis

For the measurement of Li concentration in the initial kerogen–bearing shale, isolated kerogen, and extractable organic matter, Inductively Coupled Plasma Mass Spectrometry (ICP–MS, AGILENT 8800 ICP-QQQ) was used. Where, the bulk rock was digested with mixed acid (HNO $_3$ + HCl + HF) in Teflon tubes assisted with high pressure and high temperature microwave digestion system of Milestone UltraWave; kerogen and separated organic fractions of Li were digested with HNO $_3$ + H $_2$ O $_2$ + HCl using Milestone UltraWave [20,21]. This analytical protocol utilized 0.2 N HCl to elute Li in both first and second columns while avoiding the problems induced from the usage of organic solvent, such as the degradation of resin and the residue Ca in methanol. Large columns (15 ml and 5 ml) were used to ensure that the column was not saturated for Mg $^{2+}$, Ca $^{2+}$, and other cations, which could guarantee both high Li yield (greater than 99.8 wt%) and low Na/Li ratio (less than 0.5).

After the hydrothermal reaction of kerogen–bearing shale, Li concentration in solution was measured by using ICP–MS (ICAR RQ Thermo Fisher ICP–MS). The system was flushed by 2% v/v trace grade nitric acid with the flow rate of 0.36 ml/min. The system specification was as follows: plasma power of 1,550 W; sampling depth of 5 mm; nebulizer flow of 1.03 L/min; spray chamber temperature of 2.7 °C. The stability of Li concentration measurement by the stated methodology is known to be about 0.5% of full–scale.

2.4. ToF-SIMS analysis

To identify the presence of organically and inorganically bound Li in shale rocks without chemical extraction, ToF-SIMS analysis was conducted to quantitatively understand the elemental associations inferring the molecular structures containing Li in the samples of the kerogen–bearing shale and isolated kerogen. ToF-SIMS analysis was performed using a ToF–SIMS NCS instrument, which combined a TOF. SIMS5 instrument (ION–ToF GmbH, Münster, Germany) and an in–situ Scanning Probe Microscope (NanoScan, Switzerland) at Shared Equipment Authority from Rice University.

Surface mass spectra have been obtained using a pulsed 30 keV Bi $_3^+$ ions (with a measured current of 0.15 pA) as primary probe for analyzing a field of view of $500 \times 500 \ \mu m^2$, with a raster of 128×128 pixels. A charge compensation with an electron flood gun has been applied during the analysis. An adjustment of the charge effects has been operated using the most adapted surface potential as a function of the detected polarity for both positive and negative polarities. The cycle

Table 1Major cation compositions of Marcellus Shale brines.

Cation		Concentrations in sample 1 [ppm] (Well location: 41.7279, -76.9898)	Concentrations in sample 2 [ppm] (Well location: 41.9754, -76.1347)
	Li ⁺	139	98
	Na ⁺	30,874	63,4412
	Ca ²⁺	333,112	289,724
	K^+	640.5	16,956
	Mg^{2+}	3,316	2,918

Table 2Li concentrations in Oriskany Sandstone, Devonian System, Appalachian Basin [34].

Well name	Well location	Depth to top [m]	Li concentration [ppm]
ED-82-37	39.9714, -79.0914	2,694	105
ED-82-38	39.9411, -79.1194	2,676	277
ED-82-39	39.9336, -79.1106	2,697	315
ED-82-40	40.0417, -78.9167	2,604	315
OHIO_2545	39.7417, -81.6559	1,162	167
OHIO_3477	39.6528, -81.5181	1,311	173
OHIO_65-88	41.9078, -80.7324	494	141
OHIO_709	41.8211, -81.0039	497	148
PENN_TULLY_1	42.0731, -80.0620	609	187
PENN_TULLY_45	40.1797, -79.4350	2,236	219
PENN_WEST_1203	42.0786, -80.0872	609	187

Table 3Elemental concentrations of trace elements in the initial kerogen–bearing shale of Green River Shale obtained with ICP–MS.

Element	Concentration [μg/g, ppm]	Element	Concentration [μg/g, ppm]
Li	142.4	Cs	5.91
Be	1.21	Ba	415.30
В	64.77	La	20.13
Al	36,129	Ce	37.22
Sc	4.37	Pr	4.15
Ti	1594.60	Nd	14.82
V	144.81	Sm	2.58
Cr	39.57	Eu	0.52
Mn	210.03	Gd	2.35
Co	14.26	Tb	0.31
Ni	36.53	Dy	1.75
Cu	59.44	Но	0.34
Zn	78.10	Er	1.01
Ga	9.53	Tm	0.14
Rb	105.89	Yb	0.97
Sr	459.01	Lu	0.15
Y	8.94	Hf	1.58
Zr	48.96	Ta	0.47
Nb	7.29	Re	1178.23
Mo	52.88	Pb	50.71
Cd	1.14	Th	4.88
Sn	1.05	U	4.03
Sb	3.84		

time was fixed to 90 μ s (corresponding to m/z=0—734 a.m.u mass range). The mass spectra have been collected by limiting the acquisition to the primary ion dose density of 10^{12} ions/cm² for respecting the static limit.

For the ToF–SIMS chemical mapping analysis of composite cathodes, the measurements were conducted by using a pulsed 60 keV Bi $_3^{++}$ ions (with a measured current of 0.02 pA) configurated in high lateral resolution for imaging a field of view of $500\times500~\mu\text{m}^2$, in both polarities, negative and positive, with a raster of 2,048 \times 2,048 pixels, and then the image raster has been binned by a factor 64 to enhance the signal–to–noise ratio. An appropriate adjustment of the charge effects has been operated. The cycle time was fixed to 50 μs (corresponding to m/z=0–227 a.m.u mass range).

Data from mass spectra have been normalized by the collected total ion intensity to standardize the signals from each characteristic ions, which permits to compare the ion intensity (a.u.) for the given ion, Li⁺, between the bulk rock samples of Green River Shale and the isolated kerogen samples. Using the similar approach, ion mappings have been normalized by using the total ion intensity for each pixel. The normalized ion images could then display the local variations from the analyzed regions. The approximate measurement error of ion intensity is known to be about 5%.

2.5. Hydrothermal reaction

To elucidate the fluid—rock interactions resulting in Li release from solid phase to fluid, 1 g of homogenized powder sample of kerogen—bearing shale (immature Green River Shale) and 30 ml of hydrothermal fluid were employed for each experiment of hydrothermal reactions. The hydrothermal liquids include deionized (DI) water, and solutions of individual KCl, MgCl₂, CaCl₂, and NaCl with various concentrations (0.01 M, 0.05 M, and 0.1 M). The detailed experimental conditions of 36 hydrothermal reaction cases are presented in the section 3. The samples were placed into high pressure—high temperature autoclave reactor of 50 ml—volume capacity, put into the mechanical convection oven (Thermo Scientific Heratherm OMH60-S-SS), and kept for 72 h.

2.6. BET sorption analysis

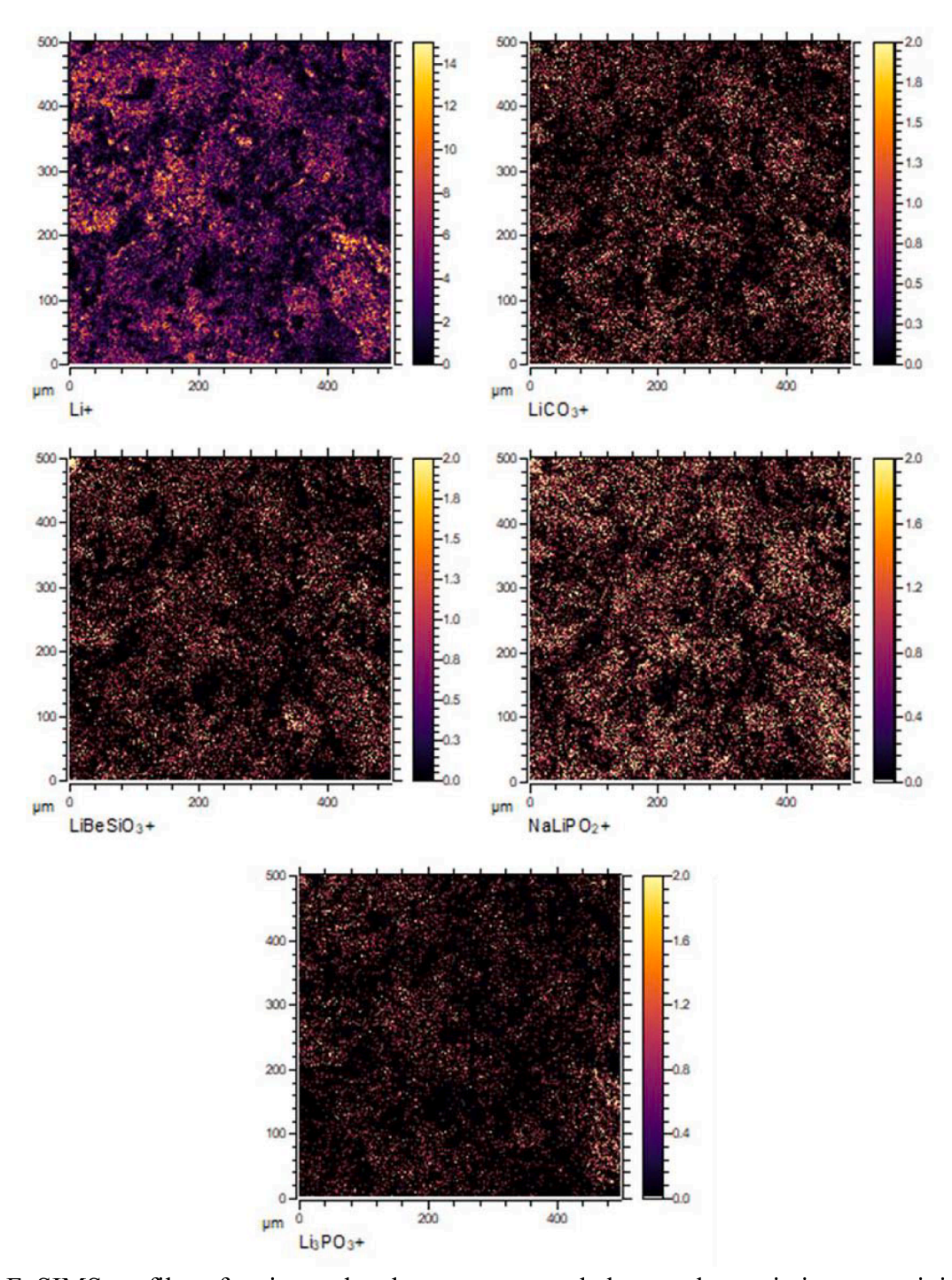
The surface and physical properties of the Green River Shale were measured by Quantachrome NOVATouch BET Sorption Analyzer with nitrogen as adsorption gas, to quantify the specific surface area of rock for the derivation of reaction rate constants. The samples were ground to $\sim 10~\mu m$ size, and the sample weight was chosen to make the expected total specific surface area of $10{-}20~m^2$. After three hours of degassing at $200~^\circ C$ with nitrogen gas, the sample weight was measured as 0.5540~g. After the degassing, adsorption–desorption analysis was implemented at the temperature of $-200~^\circ C$ for 12~h. Relative pressure resolution is known to be $1.5~\times~10^{-7} P/P_0$.

2.7. Calculation of reaction rate constants

Reaction rate constants were calculated with the experimental results, which would be used as input parameters of numerical modeling of release, transport, and accumulation of Li in shale brines. The ion exchange reactions take place between the particles of kerogen–bearing shale and various solutions of KCl, MgCl₂, CaCl₂, and NaCl, which are represented by the following reactions in Eqs. (1)-(4). Only the reactions in forward direction occur, because of the low ion activity product. Thereby, cation exchange between Li⁺ in solid as an interlayer cation of clay and another cation (i.e., K⁺, Mg²⁺, Ca²⁺, and Na²⁺) dissolved in pore fluid occurs in each reaction of Eqs. (1)-(4). In the geologic systems, the small ionic size of Li (182 pm) makes it easily dislodged from minerals through cation exchange as well as effortlessly dissolved in the brines of geologic systems [22].

$$K(a) + Li(s) \rightarrow Li(a) + K(s)$$
 (1)

$$Mg(a) + 2Li(s) \rightarrow 2Li(a) + Mg(s)$$
 (2)



(a) ToF–SIMS profiles of major molecular structures and elemental associations containing Li in the kerogen–bearing shale.

Fig. 1. Major molecular structures and elemental associations containing Li in the kerogen-bearing shale (bulk rock) and isolated kerogen of Green River Shale, obtained with ToF-SIMS.

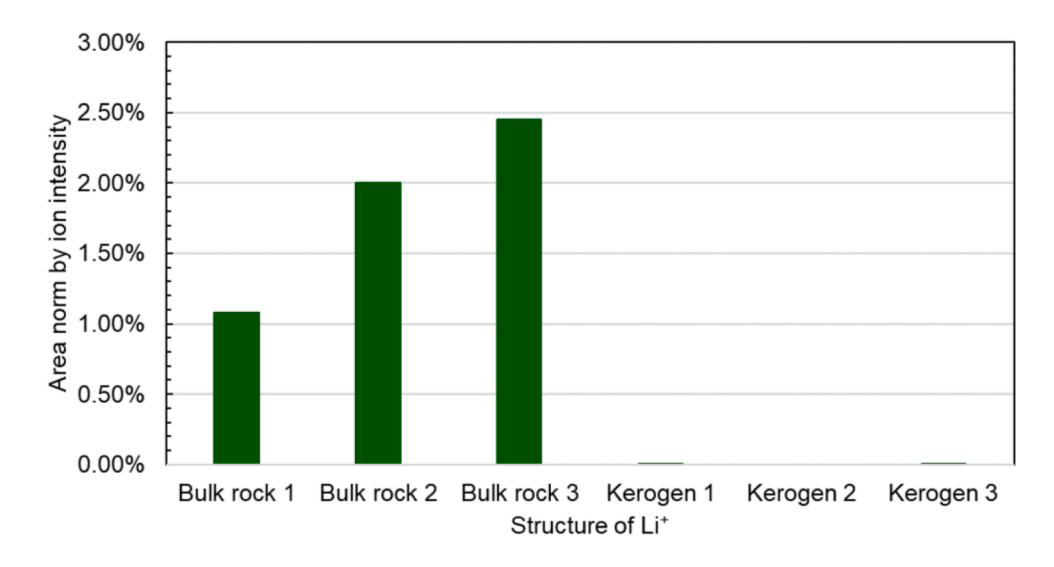
$$Ca(a) + 2Li(s) \rightarrow 2Li(a) + Ca(s)$$
 (3)

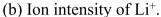
$$Na(a) + Li(s) \rightarrow Li(a) + Na(s)$$
 (4)

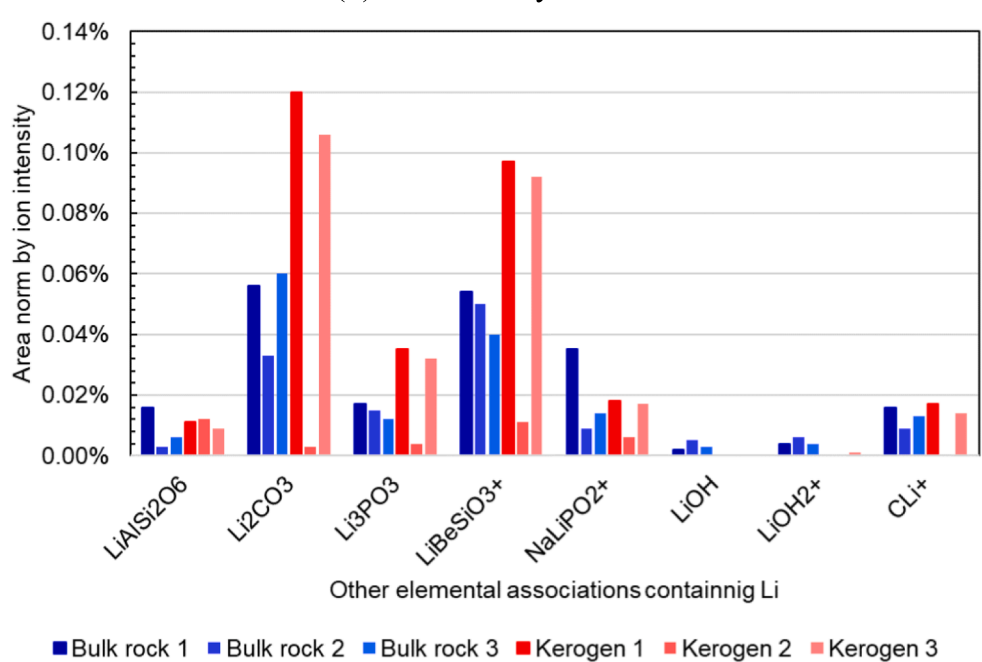
where a and s indicate aqueous phase and solid phase, respectively. If the reactions are described in the general format of the following Eq. (5), the conversion rate of Li in solid and cation in solution is calculated as in the following Eq. (6), with the assumption of first–order dependence on the reactant concentration in solution [23].

$$A(a) + bLi(s) \rightarrow bLi(a) + A(s)$$
(5)

$$-r_{A} = -\frac{1}{V} \frac{dN_{A}}{dt} = -\frac{1}{bV} \frac{dN_{Li}}{dt} = k'SC'_{A}$$
 (6)





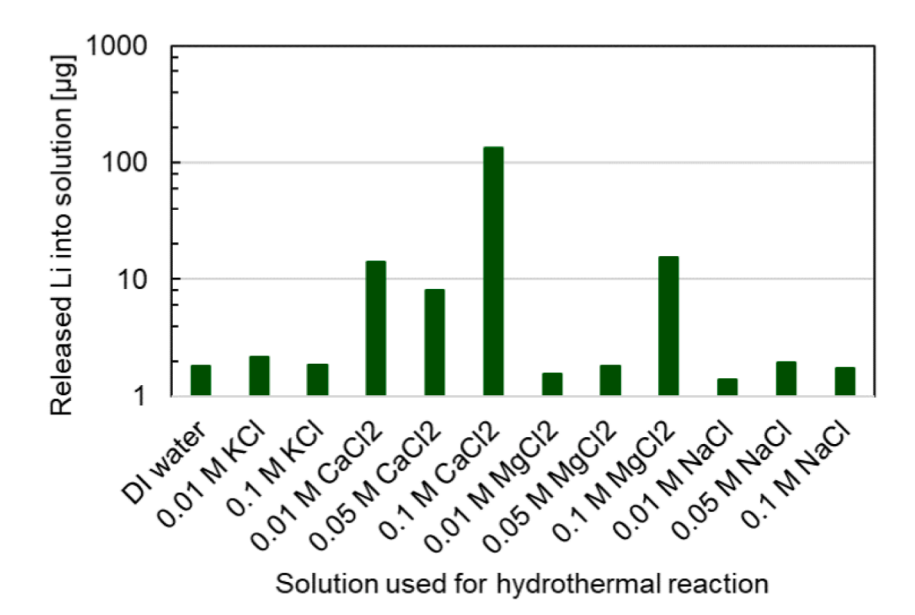


(c) Ion intensity of other molecular structures and elemental associations containing Li.

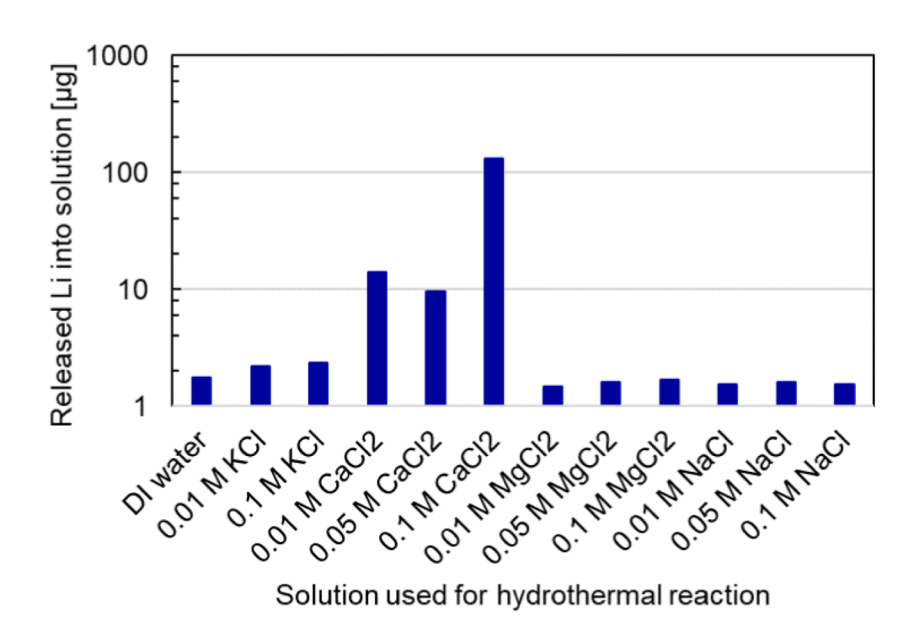
Fig. 1. (continued).

Table 4
Major molecular structures and elemental associations containing Li in the kerogen–bearing shale and isolated kerogen of Green River Shale obtained with ToF–SIMS.

Molecular	Area norm by ion intensity statistics							
Structure/ Elemental Association	Bulk rock 1	Bulk rock 2	Bulk rock 3	Kerogen 1	Kerogen 2	Kerogen 3		
Li ⁺	1.080%	2.000%	2.450%	0.001%	0.000%	0.002%		
LiAlSi ₂ O ₆	0.016%	0.003%	0.006%	0.011%	0.012%	0.009%		
Li ₂ CO ₃	0.056%	0.033%	0.060%	0.120%	0.003%	0.106%		
Li ₃ PO ₃	0.017%	0.015%	0.012%	0.035%	0.004%	0.032%		
LiBeSiO ₃ ⁺	0.054%	0.050%	0.040%	0.097%	0.011%	0.092%		
NaLiPO ₂ ⁺	0.035%	0.009%	0.014%	0.018%	0.006%	0.017%		
LiOH	0.002%	0.005%	0.003%	0.000%	0.000%	0.000%		
LiOH ₂ ⁺	0.004%	0.006%	0.004%	0.000%	0.000%	0.001%		
CLi ⁺	0.016%	0.009%	0.013%	0.017%	0.000%	0.014%		



(a) Hydrothermal reaction condition: 130 °C, 0.270 MPa.



(b) Hydrothermal reaction condition: 165 °C, 0.701 MPa.

Fig. 2. Masses of released Li into solution during hydrothermal reactions with respect to the different conditions of temperature and pressure.

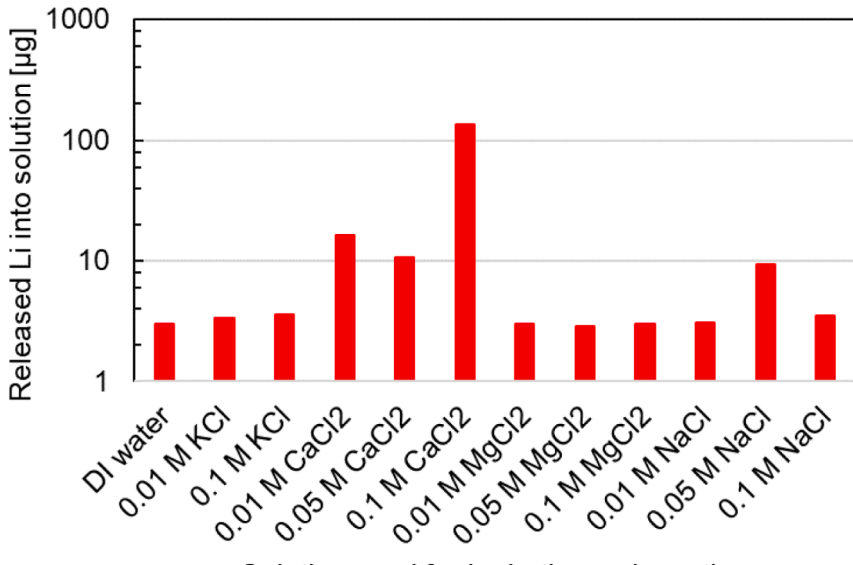
where r_A [mol/m³-s] is the reaction rate; V [m³] is the particle volume; N_A and N_{Li} [mol] are the number of moles for cation in solution and Li in rock, respectively; k' [m/s] is the reaction rate constant; S [m²/m³] is the interfacial surface area; C_A [mol/m³] is the concentration of reacting cation in solution. Reaction rate constant at 25 °C (K_{25}) [mole/m²-s] is calculated by using the following equation of temperature dependence [24–26].

$$K = K_{25} \exp \left[-\frac{E_a}{R} \left(\frac{1}{T} - \frac{1}{298.15} \right) \right]$$
 (7)

where K [mole/m²-s] is the reaction rate constant at temperature T; E_a [J/mole] is the activation energy; R [J/mole-K] is the gas constant.

2.8. Basin-scale modeling of release, transport, and accumulation of Li in shale brines

To numerically model the release, transport, and accumulation of Li in shale brines, we have used a 3D multiphase reactive—transport code, TOUGHREACT, which is based on TOUGH2 simulating a wide variety of problems in geologic media [26]. This numerical code has been successfully used for a couple of decades to model various geochemical processes in diverse subsurface environments [27–32]. The model simulates the multiphase and multicomponent fluid flow with the consideration of varying and changing system temperature, where diverse chemical reactions such as mineral—fluid interactions, aqueous phase reactions, and/or gaseous phase reactions occur.



Solution used for hydrothermal reaction

(c) Hydrothermal reaction condition: 200 °C, 1.555 MPa.

Fig. 2. (continued).

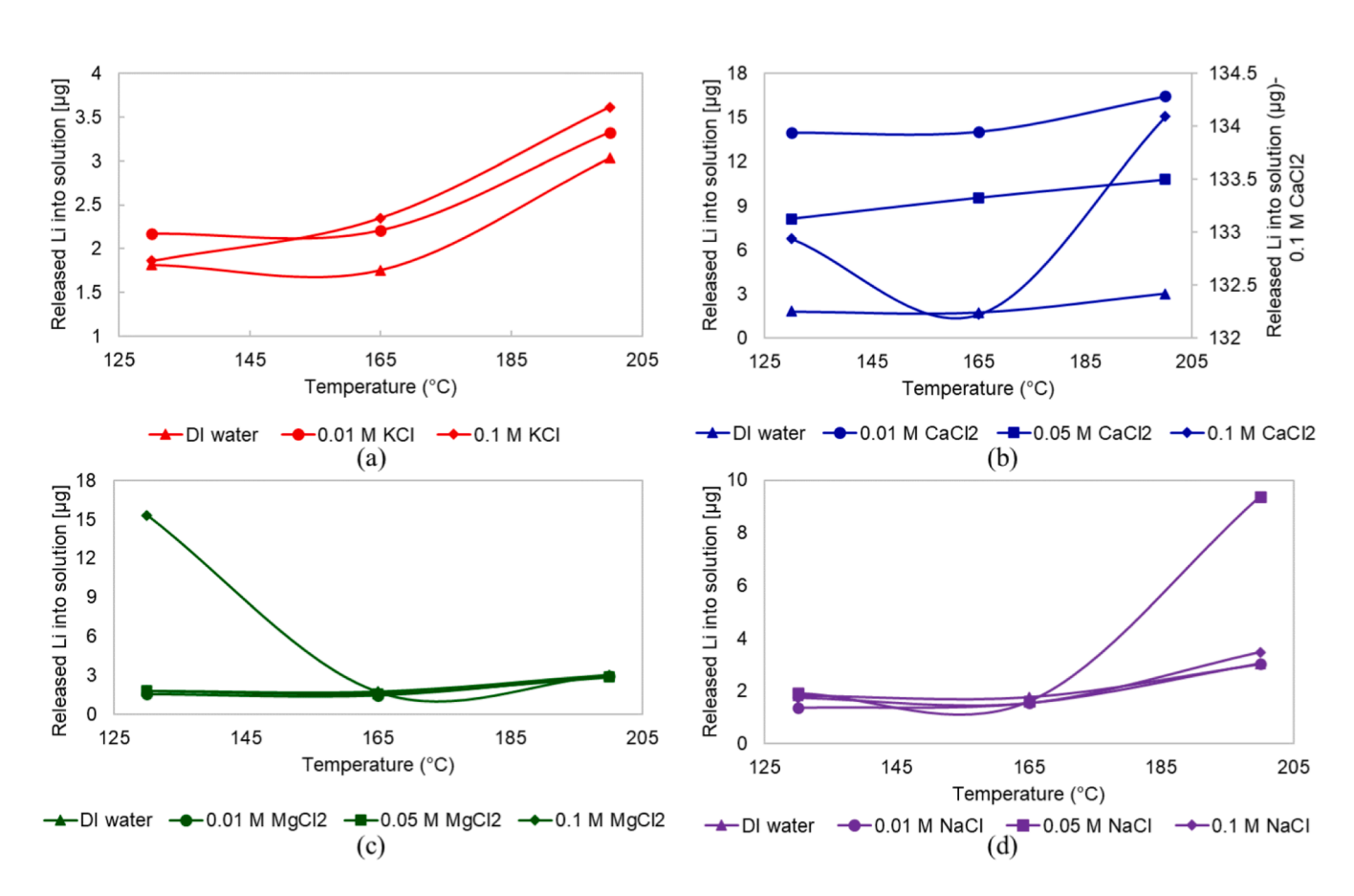


Fig. 3. Masses of released Li into solution during hydrothermal reactions with respect to different hydrothermal solutions. (a) KCl, (b) CaCl₂, (c) MgCl₂, (d) NaCl.

Details about the numerical codes solving the fluid flow equation (Darcy equation), mass-balance equation (advection-diffusion equation), energy-balance equation, and kinetic mineral dissolution and precipitation equation are described in the reference [26]. The basic

formats of these equations are presented as follows.

$$F_{\beta} = -\frac{kkr_{\beta}\rho_{\beta}}{\mu_{\beta}} \left(\nabla P_{\beta} - \rho_{\beta} \mathbf{g} \right) \tag{8}$$

Table 5Experimental cases of hydrothermal reactions for 72 h and results of released Li into fluid after hydrothermal reactions.

Case	Temperature [°C], Pressure [MPa]	Hydrothermal solution	Concentration of solution [M]	Released Li into fluid [μg]	Percentage of released Li into fluid [wt%]
1	130, 0.270	DI water	0.00	1.8172	1.2761%
2	130, 0.270	KCl	0.01	2.1670	1.5218%
3	130, 0.270	KC1	0.10	1.8619	1.3075%
4	130, 0.270	CaCl ₂	0.01	13.949	9.7957%
5	130, 0.270	CaCl ₂	0.05	8.1096	5.6950%
6	130, 0.270	CaCl ₂	0.10	132.94	93.356%
7	130, 0.270	$MgCl_2$	0.01	1.5637	1.0981%
8	130, 0.270	$MgCl_2$	0.05	1.8176	1.2764%
9	130, 0.270	MgCl ₂	0.10	15.308	10.750%
10	130, 0.270	NaCl	0.01	1.3779	0.9676%
11	130, 0.270	NaCl	0.05	1.9305	1.3557%
12	130, 0.270	NaCl	0.10	1.7386	1.2209%
13	165, 0.701	DI water	0.00	1.7576	1.2342%
14	165, 0.701	KCl	0.01	2.2064	1.5495%
15	165, 0.701	KCl	0.10	2.3516	1.6514%
16	165, 0.701	CaCl ₂	0.01	14.005	9.8349%
17	165, 0.701	CaCl ₂	0.05	9.5589	6.7127%
18	165, 0.701	CaCl ₂	0.10	132.22	92.853%
19	165, 0.701	$MgCl_2$	0.01	1.4666	1.0299%
20	165, 0.701	MgCl ₂	0.05	1.6172	1.1357%
21	165, 0.701	MgCl ₂	0.10	1.7028	1.1958%
22	165, 0.701	NaCl	0.01	1.5472	1.0865%
23	165, 0.701	NaCl	0.05	1.6111	1.1320%
24	165, 0.701	NaCl	0.10	1.5362	1.0788%
25	200, 1.555	DI water	0.00	3.0287	2.1269%
26	200, 1.555	KCl	0.01	3.3233	2.3337%
27	200, 1.555	KCl	0.10	3.6087	2.5342%
28	200, 1.555	CaCl ₂	0.01	16.435	11.542%
29	200, 1.555	CaCl ₂	0.05	10.805	7.5879%
30	200, 1.555	CaCl ₂	0.10	134.09	94.165%
31	200, 1.555	MgCl ₂	0.01	2.9742	2.0886%
32	200, 1.555	MgCl ₂	0.05	2.8930	2.0316%
33	200, 1.555	MgCl ₂	0.10	2.9944	2.1028%
34	200, 1.555	NaCl	0.01	3.0409	2.1354%
35	200, 1.555	NaCl	0.05	9.3834	6.5895%
36	200, 1.555	NaCl	0.10	3.4807	2.4443%

Table 6BET sorption analysis results of kerogen-bearing shale.

BET surface area [m²/ g]	Sample weight [g]	Average particle radius [nm]	Average pore radius [nm]	Total pore volume [cc/g]	Skeletal density [g/cc]
1.3887	0.5540	9.8197×10^{2}	3.5034	2.426×10^{-3}	2.2

Table 7Reaction rate constants for Li release from rock with each solution at different hydrothermal temperatures.

Temperature	Reaction rate constants [m/s]				
[°C]	KCl solution	CaCl ₂ solution	MgCl ₂ solution	NaCl solution	
135	4.7084×10^{-14}	1.9251×10^{-13}	2.3063×10^{-14}	2.5858×10^{-14}	
160	4.8852×10^{-14}	1.9434×10^{-13}	1.3074×10^{-14}	2.6999×10^{-14}	
200	7.3713×10^{-14}	2.1346×10^{-13}	2.5692×10^{-14}	7.0295×10^{-14}	
	Reaction rate constants at 25 °C (K ₂₅) [mole/r		ı ² -s]		
	4.4859×10^{-13}	1.7610×10^{-12}	1.8654×10^{-13}	2.6716×10^{-13}	

$$\frac{\partial M_{\kappa}}{\partial t} = -\nabla F_{\kappa} + q_{\kappa} \tag{9}$$

$$\frac{\partial M_{heat}}{\partial t} = -\nabla F_{heat} + q_{heat} \tag{10}$$

$$r = KA \left| 1 - \left(\frac{K}{Q} \right)^{\theta} \right|^{\eta} C_A \tag{11}$$

In the fluid flow equation (Eq. (8)), F_{β} is the phase flow; kkr_{β} is the phase permeability; ∇P_{β} is the phase pressure gradient; ρ_{β} is the phase density; \mathbf{g} is the gravity vector. In the mass–balance equation (Eq. (9)), $\frac{\partial M_{\kappa}}{\partial t}$ is the component mass change with respect to time; ∇F_{κ} is the component mass flux by Darcy flow and diffusion; q_{κ} is the component source/sink. In the energy–balance equation (Eq. (10)), $\frac{\partial M_{heat}}{\partial t}$ is the heat accumulation with respect to time; ∇F_{heat} is the heat flux by conduction and convection of heat; q_{heat} is the heat source/sink. In the kinetic mineral dissolution and precipitation equation (Eq. (11)), r is the kinetic reaction rate; K is the time–dependent reaction rate constant (Eq. (7)); K0 is the reactive surface area of mineral; K1 is the equilibrium constant for mineral–fluid reaction; K2 is the reaction quotient; exponents K3 and K4 are fitting parameters, which were assumed as 1 in the modeling of this study; K4 [M] is the concentration of reacting cation in solution.

For the computational feasibility, we introduced the concept of geologic time (t_{geol}) and simulation time (t_{sim}) in modeling. By equating the reaction rate multiplied by time in each scale (Eq. (12) and Eq. (13)), we could define the C_A in simulation time scale (Eq. (14)) [18].

$$r_{\text{geol}} \bullet t_{\text{geol}} = KA \left| 1 - \left(\frac{K}{Q} \right)^{\theta} \right|^{\eta} C_{A,\text{geol}} \bullet t_{\text{geol}}$$
 (12)

 Table 8

 Initial aqueous and mineral compositions in modeling.

•		U		
Aqueous species	Initial composition* [M]	Mineral components	Initial composition [vol %]	k_{25} [mol/m ² -s], E_a [kJ/mol], A [m ² /g]
H ⁺ Ca ²⁺ Mg ²⁺	10 ⁻⁸	Li-montmorillonite	2.25	k_{25} : 4.4859 \times 10 $^{-13}$ (K+ dominancy); 1.7610 \times 10 $^{-12}$ (Ca $^{2+}$ dominancy); 1.8654 \times 10 $^{-13}$ (Mg $^{2+}$ dominancy); 2.6716 \times 10 $^{-13}$ (Na $^{+}$ dominancy), $E_a=53.5,$ $A=84.0$
Na ⁺ Li ⁺		K, Ca, Mg, Na–montmorillonite	0	Same as Li-montmorillonite
K^+ $Cl^ SiO_2(aq)$ $HCO^3-SO_4^2-AlO_2^-$		Other minerals	97.75%	Assumed to be inactive (No reactions occur.)

^{*} The initial aqueous compositions before geologic time from present time are unknown, and they have been assumed to be insignificant given that we consider the initial condition before fluid–rock interactions. The initial composition of each dominant cation (among K⁺, Ca²⁺, Mg²⁺, and Na⁺) in each case was 0.01 M.

$$r_{\text{sim}} \bullet t_{\text{sim}} = KA \left| 1 - \left(\frac{K}{Q} \right)^{\theta} \right|^{\eta} C_{A,\text{sim}} \bullet t_{\text{sim}}$$
 (13)

$$C_{A,\text{sim}} = \frac{C_{A,\text{geol}} \bullet t_{\text{geol}}}{t_{\text{sim}}} \tag{14}$$

In our modeling, we used $C_{A,\rm sim}$ of 0.01 M with the reaction completion time ($t_{\rm sim}=0.1$ year) of forward reactions (dissolution of Li–montmorillonite and precipitation of Ca–montmorillonite) of the fastest case with Ca²⁺ dominancy in pore fluid, given the approximate $t_{\rm geol}$ of 0.1 million years and $C_{A,\rm geol}$ of 10^{-8} M. Similarly, we adjusted the fluid diffusivity in the simulation time scale by equating the diffusivity multiplied by time in each scale (Eq. (15) and Eq. (16)), and we could define the permeability (k) in simulation time scale (Eq. (17)) [18].

$$\eta_{\text{geol}} \bullet t_{\text{geol}} = \frac{k_{\text{geol}}}{\varnothing \mu c_{i}} \bullet t_{\text{geol}}$$
(15)

$$\eta_{\text{sim}} \bullet t_{\text{sim}} = \frac{K_{\text{sim}}}{\emptyset \mu c_t} \bullet t_{\text{sim}} \tag{16}$$

$$k_{\rm sim} = \frac{k_{\rm geol} \bullet t_{\rm geol}}{t_{\rm sim}} \tag{17}$$

In our modeling, we used $k_{\rm sim}$ of 1,000 md, by considering $t_{\rm geol}=0.1$ million years, $t_{\rm sim}=0.1$ year, and $k_{\rm geol}=1$ µd, respectively.

3. Results and discussion

3.1. Presence of Li in the produced water from shale containing mature kerogen

Ion chromatography analysis was conducted to measure the concentrations of cations including Li ion dissolved in the two samples of brines produced from Marcellus Shale containing moderately mature Type II kerogen, which was obtained in December 2020. Measured concentrations of major cations including Li ion (139 ppm and 98 ppm) in Table 1 are in the ranges of published data of produced water from Marcellus Shale [33], which are highly variant. In addition, from the published Li concentrations with the average of 203 ppm (Table 2) in Oriskany Sandstone [34], which is located deeper than Marcellus Shale in the Devonian System of Appalachian basin, the measured Li concentrations in Marcellus Shale can be seen as in a representative range. Plentiful presence of various cations (Na+, Ca2+, K+, and Mg2+) indicates their potentially significant impact on the dissolution and mineralization of Li through fluid-rock interactions. Dominantly high concentration of Ca²⁺ is noticeable, which is explained by the variable composition of carbonate minerals ranging from 3 to 58% in Marcellus Shale [35-37].

3.2. Initial presence of Li in shale containing immature kerogen

Integrative high-precision characterization of Li compositions in the isolated kerogen and kerogen-bearing bulk rock is critical to advance the fundamental knowledge of the mechanisms of the release of Li into pore fluid through the fluid-rock interactions, given that Li can be either organically bound or inorganically bound in shale rocks. The initial elemental compositions of kerogen-bearing bulk rocks and isolated kerogen were analyzed using Triple Quadrupole Inductively Coupled Plasma Mass Spectrometry (ICP-MS). The concentrations of trace elements of kerogen-bearing shale, isolated kerogen, and extractable organic matters (mainly bitumen and mature hydrocarbons) of Green River Shale are presented in Table 3 and Supplementary Tables 1 and 2. Li elemental concentration of 142.4 ppm in kerogen-bearing shale, which is in accordance with the published data of 141 ppm [15], indicates the significant amount of Li as a solid phase in immature organic-rich shale. We note that Si was not analyzed with ICP-MS, because we used a high purity quartz glass digestion tube to digest the samples with Microwave before analyzing the elements with ICP-MS. The background/contamination from the quartz tube was too high on Si to get any meaningful Si analysis in samples.

From the Supplementary Tables 1 and 2, the Li concentrations of about 1 ppm in isolated kerogen and 0.05 ppm in extractable organic matters indicate that 1) organically bound Li might have been removed during the closed-loop isolation using acids, or that 2) Li was mainly bound with inorganic minerals initially, and less than 1% of bulk rock concentrations was bound with organic matter (kerogen). To determine the validity of each hypothesis, Time-of-Flight Secondary Ion Mass Spectrometry (ToF-SIMS) analysis was implemented on the multiple samples of kerogen-bearing shale and isolated kerogen, and their results are summarized in the Supplementary Tables 3–8. As in accordance with the ICP-MS results, the bulk rock of Green River Shale contained abundant Li, while the isolated kerogen contained only insignificant amount of it. In order to determine the relative portions of organic and inorganic Li in the bulk rock of Green River Shale, ToF-SIMS was applied to analyze the various molecular structures. Fig. 1 shows the molecular structures containing Li in the samples of the kerogen-bearing shale and isolated kerogen of Green River Shale. As can be seen, Li₂CO₃ is the major molecular structure of organically bound Li followed by elementally associated LiBeSiO₃⁺, even their intensities are much lower than the one of inorganically bound Li⁺. Organically bound Li in the molecular structure of Li₂CO₃ is also supported by the presence of carbonyl stretch C = O in isolated kerogen of Green River Shale as presented in the authors' recent publication [38]. From the ToF-SIMS results, both hypotheses that 1) Li was mainly bound with inorganic minerals initially, and that 2) insignificant but some of Li might have been removed from the kerogen during the closed-loop isolation can be validated. Given that the majority of Li is presented as Li⁺ in bulk rock, it can be inferred that the most of Li in kerogen-bearing shale would be presented either as interlayer cation in clay minerals such as smectite (e.

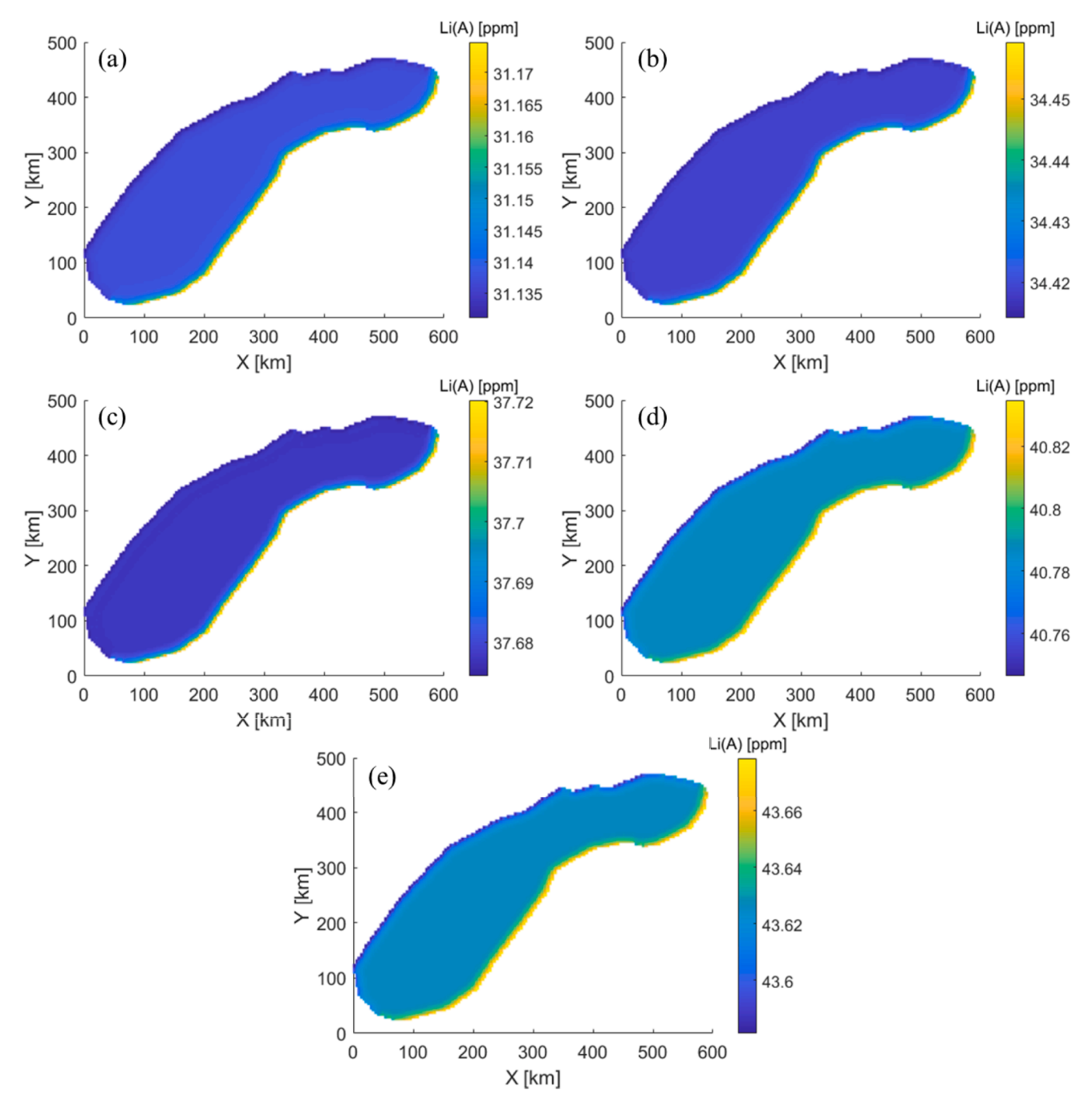


Fig. 4. Profiles of Li concentration in brine in a conceptual geologic model mimicking Marcellus Shale with K^+ dominancy in pore fluid. (a) Z (depth of the top of layer) = -1,380 m, (b) Z = -1,480 m, (c) Z = -1,580 m, (d) Z = -1,680 m, (e) Z = -1,780 m.

g., montmorillonite), bound with the minerals such as silicates and carbonates, or adsorbed to the minerals such as zeolites and clays [39,40]. The quantified results are presented in Table 4.

3.3. Release of Li into fluid

Using the homogenized powder samples of kerogen–bearing bulk rock, hydrothermal reactions under various experimental conditions were conducted. Given the major cations found from the ion chromatography analysis of produced brines from mature kerogen–bearing shale formation of Marcellus Shale (Table 1), various solutions containing Na $^+$, Ca $^{2+}$, K $^+$, and Mg $^{2+}$ cations as well as deionized water were used as hydrothermal fluids. After 72 h of hydrothermal reactions, concentrations of Li in hydrothermal solutions were measured with

ICP–MS to quantify the mass of released Li into solution and its weight percentages, as visualized in Fig. 2 and Fig. 3, respectively. Fig. 2 indicates the impact of the types of cations presenting in hydrothermal fluid. Ca^{2+} was found to be most effective for the release of Li from rock (Green River Shale) into pore fluid. This can be addressed by that fast hydration shell exchange rate of Ca^{2+} made it easier to exchange for bound Li [41,42]. This is also because that heavier element with higher ionic charge is preferable to be fixed in the interlayer of clay under humid condition by exchanging with lighter element with lower ionic charge [22,41,42]. Abundant presence of Ca^{2+} in Marcellus Shale brines in Table 1 is in accordance with the results of this hydrothermal reaction experiment, by providing the background of high Li concentration in brines. Impact of other cations of Na^+ , Mg^{2+} and K^+ on the release of Li was relatively insignificant, as controlled by hydrothermal reaction

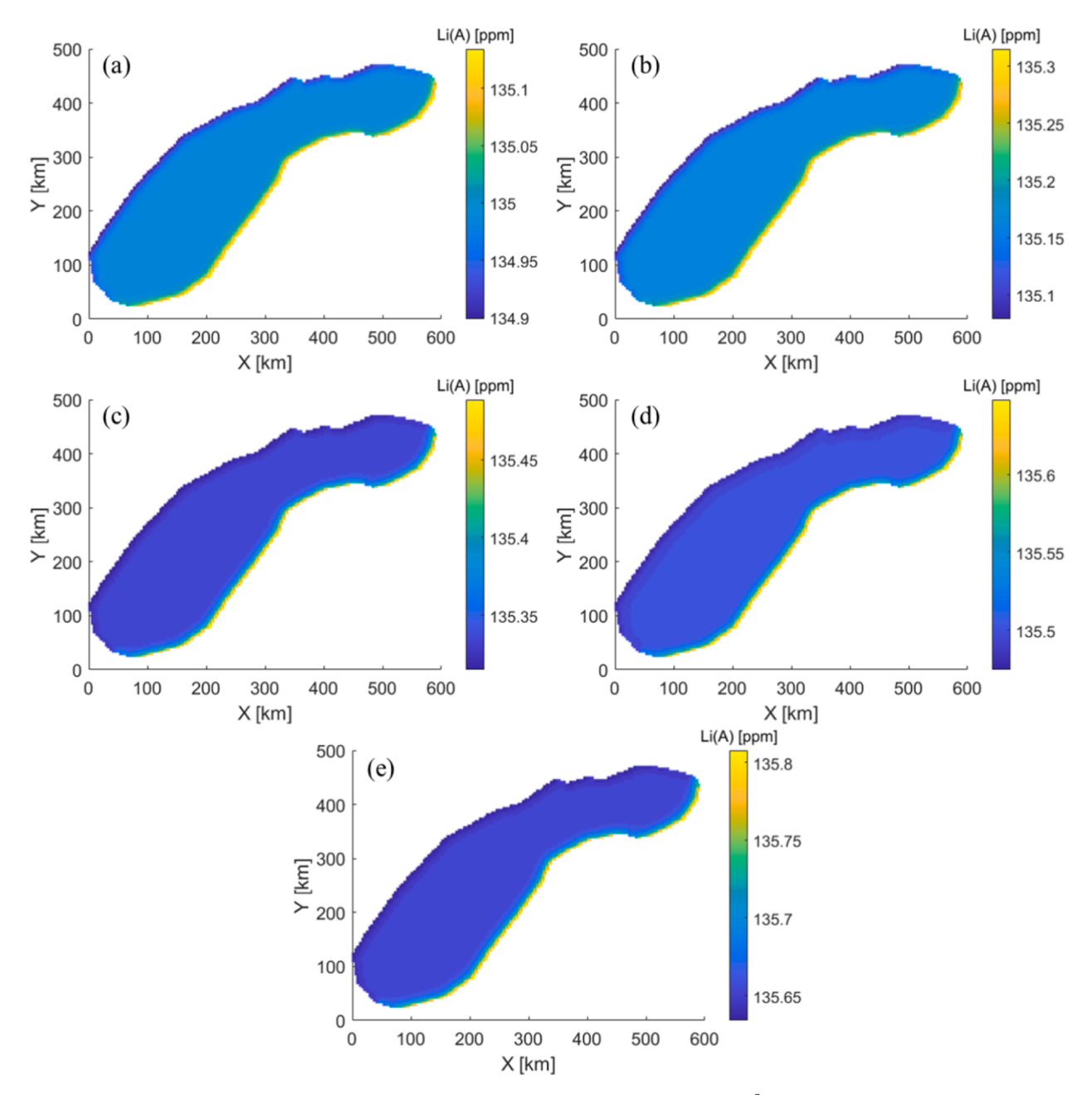


Fig. 5. Profiles of Li concentration in brine in a conceptual geologic model mimicking Marcellus Shale with Ca^{2+} dominancy in pore fluid. (a) Z (depth of the top of layer) = -1,380 m, (b) Z = -1,480 m, (c) Z = -1,580 m, (d) Z = -1,680 m, (e) Z = -1,780 m.

conditions such as temperature, pressure, and ion concentrations. As presented in the quantified results in Table 5, weight percentages of released Li from rock into fluid ranged from about 0.97% (130 $^{\circ}$ C, 0.270 MPa, 0.01 M NaCl solution) to 94% (200 $^{\circ}$ C, 1.555 MPa, 0.1 M CaCl $_{2}$ solution).

Applying the BET sorption analysis results regarding specific surface area shown in Table 6, reaction rate constants of Li release for each solution and temperature were calculated and presented in Table 7. By applying the exponential relationship of reaction rate constant at 25 °C (K_{25}) [mole/m²-s] and different various temperature, K_{25} was calculated for each temperature in each solution. Then the calculated values of K_{25} were averaged over different temperatures in each solution, as presented in Table 7. K_{25} in Ca²+ presence in solution was 1.7610 × 10^{-12 mol}/m²-s, followed by the cases of K+ presence (4.4859 × 10^{-13 mol}/m²-s), Na+ presence (2.6716 × 10^{-13 mol}/m²-s), and Mg²+ presence (1.8654 × 10^{-13 mol}/m²-s) in solution. Note that the lower value of calculated K_{25}

in the case of ${\rm Mg}^{2+}$ presence than the cases of ${\rm K}^+$ and ${\rm Na}^+$ presence was mainly caused by the higher ionic charge of ${\rm Mg}^{2+}$, which didn't necessarily mean the lower efficiency of ${\rm Mg}^{2+}$ to release Li into fluid (Fig. 2 and Fig. 3).

3.4. Modeling of release, transport, and accumulation of Li in shale brines

To investigate the transport and accumulation of released Li in shale brines, we developed a conceptual three–dimensional reactive transport model mimicking Marcellus Shale system. The model was consisted of 31,690 uniform structural elements (4,023.35 m \times 4,023.35 m \times 100 m, five layers in Z–direction) with 87,416 connections between them. The dip angle of the model was -0.8682° in S–56.3100°–E direction [43,44]. The initial model was composed of homogeneous mineral compositions with 2.25 vol% of Li–montmorillonite [45] containing about 140 ppm of Li in solid phase as found from the measurement of initial presence of Li

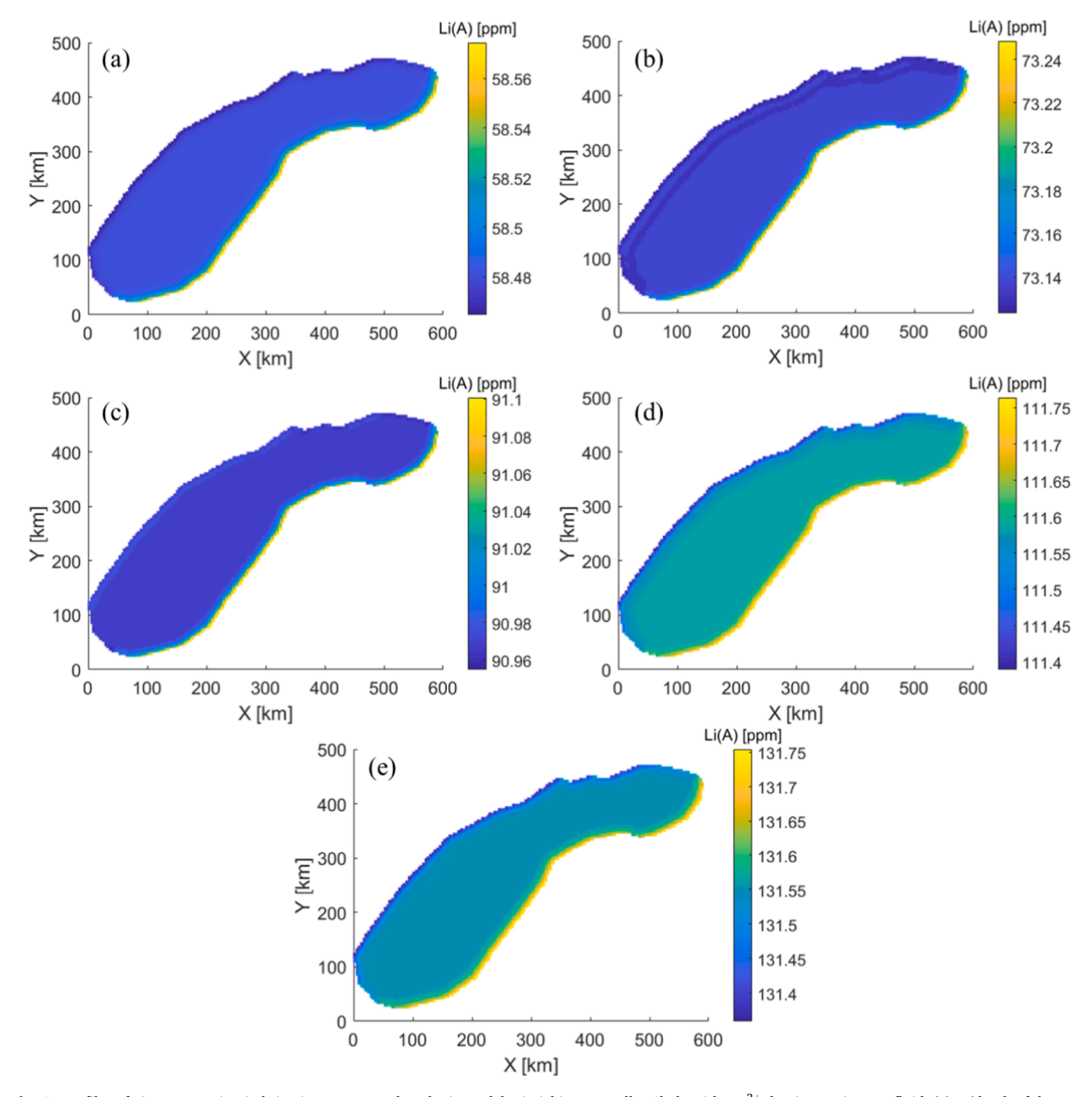


Fig. 6. Profiles of Li concentration in brine in a conceptual geologic model mimicking Marcellus Shale with Mg^{2+} dominancy in pore fluid. (a) Z (depth of the top of layer) = -1,380 m, (b) Z = -1,480 m, (c) Z = -1,580 m, (d) Z = -1,680 m, (e) Z = -1,780 m.

in shale rock with immature kerogen (Table 3). Consideration of clay mineral with interlayer, montmorillonite, as a host mineral of Li was justified by the abundant presence of Li $^+$ in minerals (section 3.2. Initial presence of Li in shale containing immature kerogen) and effectiveness of release of Li through cation exchange (section 3.3. Release of Li into fluid). Four different models were consisted with various pore fluid compositions [33,46], indicating the different dominancy of K^+ , Ca^{2+} , Mg^{2+} , and Na^+ , respectively. The initial aqueous and mineral compositions were uniform throughout the entire model, which are presented in the Table 8. The vertical distributions of pressure and temperature from the top layer to bottom layer were from 13.60 MPa to 17.52 MPa and from 74.5 °C to 85.5 °C, respectively [43]. In the modeling of mass and heat flow, no flow boundary conditions were considered. Given that

clay minerals controlling Li concentration in water depend on temperature [47–49], different temperature condition of numerical modeling (74.5–85.5 $^{\circ}\text{C}$, mainly controlled by montmorillonite) from the temperature condition of hydrothermal reaction experiments (130–200 $^{\circ}\text{C}$, mainly controlled by illite and mica) needs to be noted as a potential limitation of combining experimental results to numerical modeling in this study.

The model simulated the interaction between pore fluid containing various aqueous species and Li–montmorillonite in rock, release of Li $^+$ into pore fluid and fixation of cations—K $^+$, Ca $^{2+}$, Mg $^{2+}$, and Na $^+$ —at the interlayer of montmorillonite, and fate and transport of Li in pore fluid. As every simulation case was designed to model the forward reaction of Li release from Li–montmorillonite into pore fluid by assigning sufficient

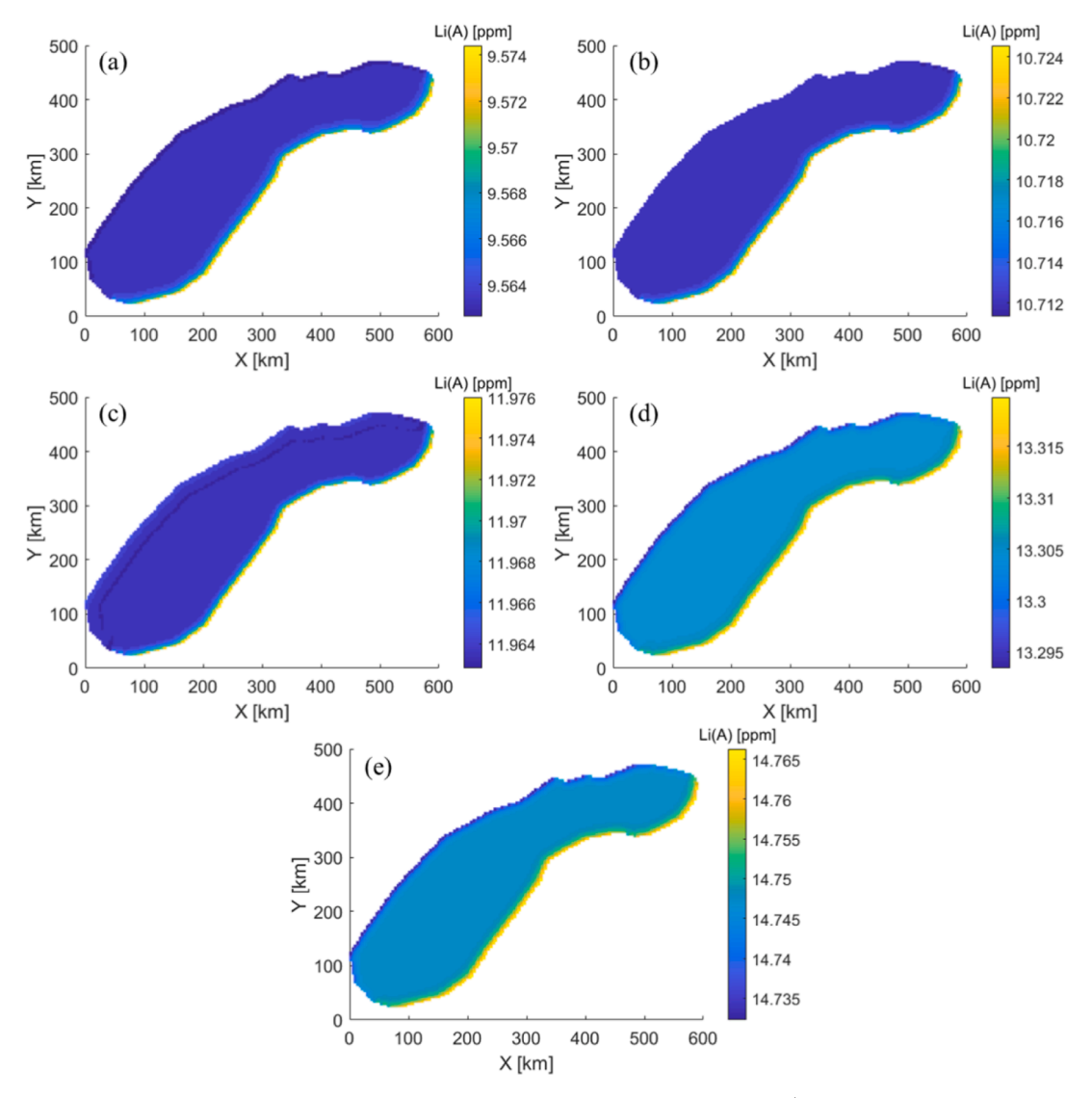


Fig. 7. Profiles of Li concentration in brine in a conceptual geologic model mimicking Marcellus Shale with Na $^+$ dominancy in pore fluid. (a) Z (depth of the top of layer) = -1,380 m, (b) Z = -1,480 m, (c) Z = -1,580 m, (d) Z = -1,680 m, (e) Z = -1,780 m.

amounts of cations in pore fluid, every simulation was continued until the completion time ($t_{sim} \approx 0.1$ year, which corresponds to $t_{opol} \approx 0.1$ million years) of forward reactions (dissolution of Li-montmorillonite and precipitation of K, Ca, Mg, or Na-montmorillonite) of the fastest case with Ca²⁺ dominancy in pore fluid. The profiles of spatial distributions of Li concentrations in brines with different dominant cations are presented in Figs. 4-7. As predictable from the results of hydrothermal reaction experiments, Li concentrations in brines were highest in the case with Ca²⁺ dominancy in pore fluid, which ranged from 134.90 ppm to 135.81 ppm (average: 135.33 ppm). Li concentrations in brines were lowest in the case with Na⁺ dominancy in pore fluid, which ranged from 9.56 ppm to 14.77 ppm (average: 12.06 ppm). In the K⁺-dominant case and Mg²⁺-dominant case, Li concentrations in brines ranged from 31.13 ppm to 43.68 ppm (average: 37.53 ppm) and from 58.46 ppm to 131.75 ppm (average: 93.15 ppm), respectively. The incomparable abundance of Ca²⁺ in Marcellus Shale brines indicates its dominancy in pore fluid, which produces the magnitude in accordance with Li concentration in brines in the computed values as in Fig. 5 (average: 135.33 ppm) with measured values as in Table 1 (139 ppm and 98 ppm).

4. Conclusions

This study demonstrates that the reliable estimation of Li resources in a new source of shale brines can be possible by the understanding of fundamental phenomena addressing release, transport, and accumulation of Li in geologic system. The main findings from this study are summarized as follows.

- The initial presence of Li in shale rocks have been experimentally characterized with ICP-MS and ToF-SIMS analyses. In the bulk shale containing immature kerogen, Li was found to be mainly bound with minerals as an interlayer cation of clay.
- The release mechanism of Li from solid to fluid was experimentally analyzed. Where, hydrothermal reaction experiments were conducted with 36 different cases of temperature, solution types, and solution concentrations. From the experiments, Ca²⁺ was found to be most effective for the release of Li from rock into pore fluid, followed by Mg²⁺, K⁺, and Na⁺.
- The release, transport, and accumulation of Li in shale brines were numerically simulated through the basin-scale modeling, as combined with the experimental findings. The modeling results

- presented the potential of Marcellus Shale brines as a source of Li, depending on the dominant cation in the system.
- The average concentration of Li in shale brines mimicking Marcellus Shale system was estimated to be about 135 ppm under Ca²⁺ dominancy in pore fluid, which showed excellent match with actually measured values from produced Marcellus Shale brines.

Our results of the estimated Li concentration in shale brines mimicking Marcellus Shales system, obtained with numerical modeling coupled with a suite of geochemical experiments and characterization, are consistent with the field observations. Our estimations clearly provide a significant role of dominant cation compositions in natural pore fluid for Li to be released from rock to fluid and subsequent fate and transport in shale brines. The estimated Li concentration of 135 ppm indicates the Li resources of about 2.97×10^5 metric tons, based on the projected produced water volume of $2,200 \times 10^9$ L from Marcellus Shale system for upcoming 73 years. Given the U.S. annual demand of 2,000 metric tons of Li, it corresponds to the potential of 150 years of Li demand in the U.S. These findings also have implications for the potential estimations of other critical elements in new types of unconventional sources (e.g., various other shale systems and geothermal systems). Beyond improving our fundamental knowledge about estimating the potential of Li supply from brines in Marcellus Shale environment, various other subsurface formations can be benefitted through our systematic understanding, and thereby it can contribute to provide diverse subsurface brines as a new sustainable source of critical minerals' supply including Li.

CRediT authorship contribution statement

Kyung Jae Lee: . Jiahui You: . Yongjun Gao: Writing – review & editing, Investigation, Data curation. Tanguy Terlier: Writing – review & editing, Investigation, Formal analysis, Data curation.

Declaration of Competing Interest

The authors declare that they have no known competing financial interests or personal relationships that could have appeared to influence the work reported in this paper.

Data availability

Data will be made available on request.

Acknowledgements

We appreciate the funding for this research from National Science Foundation under Award 2042504 (CAREER: Identifying a New Source of Lithium for Sustainable and Renewable Energy Storage). The paper was benefitted from the support of J. Casey and K. Bissada of Department of Earth and Atmospheric Sciences at the University of Houston, for letting us to utilize their laboratory facilities for elemental analysis and kerogen isolation, respectively. We also thank a company in Utah for providing Green River Shale samples, and another company in Pennsylvania for providing the produced water samples from Marcellus Shale. ToF–SIMS analysis was carried out with support provided by the National Science Foundation CBET-1626418, where it was conducted in part using the resources of the Shared Equipment Authority (SEA) at Rice University.

Appendix A. Supplementary data

Supplementary data to this article can be found online at https://doi.org/10.1016/j.fuel.2023.129629.

References

- Maisel F, Neef C, Marscheider-Weidemann F, Nissen NF. A forecast on future raw material demand and recycling potential of lithium-ion batteries in electric vehicles. Resour Conserv Recycl 2023;192:106920.
- [2] Yang S, Zhang F, Ding H, He P, Zhou H. Lithium metal extraction from seawater. Joule 2018;2(9):1648–51.
- [3] Dugamin EJ, Richard A, Cathelineau M, Boiron M-C, Despinois F, Brisset A. Groundwater in sedimentary basins as potential lithium resource: A global prospective study. Sci Rep 2021;11(1):21091.
- [4] Martin G, Rentsch L, Höck M, Bertau M. Lithium market research-global supply, future demand and price development. Energy Storage Mater 2017;6:171-9.
- [5] McCarthy K, Rojas K, Niemann M, Palmowski D, Peters K, Stankiewicz A. Basic petroleum geochemistry for source rock evaluation. Oilfield Review 2011;23(2): 32–43
- [6] De Silva P, Simons S, Stevens P, Philip L. A comparison of North American shale plays with emerging non-marine shale plays in Australia. Mar Pet Geol 2015;67: 16–29.
- [7] Jang E, Jang Y, Chung E. Lithium recovery from shale gas produced water using solvent extraction. Appl Geochem 2017;78:343–50.
- [8] Scanlon BR, Reedy RC, Xu P, Engle M, Nicot J, Yoxtheimer D, et al. Can we beneficially reuse produced water from oil and gas extraction in the US? Sci Total Environ 2020;717:137085
- [9] Veil J. US produced water volumes and management practices in 2012. Groundwater Protection Council 2015.
- [10] USGS. Lithium Data Sheet Mineral Commodity Summaries 2020. 2020.
- [11] Vera ML, Torres WR, Galli CI, Chagnes A, Flexer V. Environmental impact of direct lithium extraction from brines. Nature Reviews Earth & Environment 2023;4(3): 149–65.
- [12] Xu W, Liu D, Liu X, Wang D, He L, Zhao Z. Highly selective and efficient lithium extraction from brines by constructing a novel multiple-crack-porous LiFePO4/ FePO4 electrode. Desalination 2023;546:116188.
- [13] Liu G, Zhao Z, Ghahreman A. Novel approaches for lithium extraction from salt-lake brines: A review. Hydrometall 2019;187:81–100.
- [14] Sun Y, Wang Q, Wang Y, Yun R, Xiang X. Recent advances in magnesium/lithium separation and lithium extraction technologies from salt lake brine. Sep Purif Technol 2021;256:117807.
- [15] Jochum KP, Nohl U, Herwig K, Lammel E, Stoll B, Hofmann AW. GeoReM: a new geochemical database for reference materials and isotopic standards. Geostand Geoanal Res 2005;29(3):333–8.
- [16] Katz B. The Green River Shale: an Eocene carbonate lacustrine source rock. Petroleum source rocks Springer 1995:309–24.
- [17] Feng J. Source rock characterization of the Green River oil shale, Piceance Creek basin, Colorado. Colorado School of Mines. Arthur Lakes Library; 2011.
- 18] Lee KJ. Potential of petroleum source rock brines as a New Source of Lithium: Insights from basin-scale modeling and local sensitivity analysis. Energy Rep 2022; 8:56-68
- [19] Sun T, Bake KD, Craddock PR, Gunawan B, Darnell LM, Bissada KK, et al. Acid demineralization with pyrite removal and critical point drying for kerogen microstructural analysis. Fuel 2019;253:266–72.
- [20] Yang W, Casey JF, Gao Y. A new sample preparation method for crude or fuel oils by mineralization utilizing single reaction chamber microwave for broader multielement analysis by ICP techniques. Fuel 2017;206:64–79.
- [21] Gao Y, Casey JF, Bernardo LM, Yang W, Bissada KA. Vanadium isotope composition of crude oil: effects of source, maturation and biodegradation. Geol Soc Lond Spec Publ 2018;468(1):83–103.
- [22] Vine JD. Lithium in sediments and brines—how, why, and where to search. J Res US Geol Surv 1975;3(4):479–85.
- [23] Kimura S, Takagi Y, Tone S, Otake T. A rate equation for gas-solid reactions accounting for the effect of solid structure and its application. J Chem Eng Jpn 1981;14(6):456-61.
- [24] Lasaga AC, Soler JM, Ganor J, Burch TE, Nagy KL. Chemical weathering rate laws and global geochemical cycles. Geochim Cosmochim Acta 1994;58(10):2361–86.
- [25] Xu T, Spycher N, Sonnenthal E, Zhang G, Zheng L, Pruess K. TOUGHREACT Version 2.0: A simulator for subsurface reactive transport under non-isothermal multiphase flow conditions. Comput Geosci 2011;37(6):763–74.
- [26] Sonnenthal E, Spycher N, Xu T, Zheng L. TOUGHREACT V4. 12-OMP and TReactMech V1. 0 Geochemical and Reactive-Transport User Guide. 2021.
- [27] Audigane P, Gaus I, Pruess K, Xu T. A long term 2D vertical modelling study of CO2 storage at Sleipner (North Sea) using TOUGHREACT. Proceedings, TOUGH Symposium. 2006: 8.
- [28] Seol Y, Lee K-K. Application of TOUGHREACT to performance evaluations of geothermal heat pump systems. Geosci J 2007;11(1):83–91.
- [29] Barkouki T, Martinez B, Mortensen B, Weathers T, De Jong J, Ginn T, et al. Forward and inverse bio-geochemical modeling of microbially induced calcite precipitation in half-meter column experiments. Transp Porous Media 2011;90(1):23–39.
- [30] Shevalier M, Nightingale M, Mayer B, Hutcheon I. TOUGHREACT modeling of the fate of CO2 injected into a H2S containing saline aquifer: The example of the Wabamum Area Sequestration Project (WASP). Energy Procedia 2011;4:4403–10.
- [31] Klunk MA, Damiani LH, Feller G, Conceição RV, Abel M, De Ros LF. Geochemical modeling of diagenetic reactions in Snorre Field reservoir sandstones: a comparative study of computer codes. Braz J Geol 2015;45:29–40.
- [32] Shabani B, Vilcáez J. TOUGHREACT-CO2Bio-A new module to simulate geological carbon storage under biotic conditions (Part 1): The multiphase flow of CO2-CH4-H2-H2S gas mixtures. J Nat Gas Sci Eng 2019;63:85-94.

- [33] Barbot E, Vidic NS, Gregory KB, Vidic RD. Spatial and temporal correlation of water quality parameters of produced waters from Devonian-age shale following hydraulic fracturing. Environ Sci Tech 2013;47(6):2562–9.
- [34] Skeen JC. Basin analysis and aqueous chemistry of fluids in the Oriskany Sandstone. USA: Appalachian Basin; 2010.
- [35] Phan TT, Capo RC, Stewart BW, Graney JR, Johnson JD, Sharma S, et al. Trace metal distribution and mobility in drill cuttings and produced waters from Marcellus Shale gas extraction: Uranium, arsenic, barium. Appl Geochem 2015;60: 89–103.
- [36] Ferguson B, Agrawal V, Sharma S, Hakala JA, Xiong W. Effects of Carbonate Minerals on Shale-Hydraulic Fracturing Fluid Interactions in the Marcellus Shale. Frontiers. Earth Sci 2021::1072.
- [37] Khalil R, Emadi H, Altawati F. Investigating the effect of matrix acidizing injection pressure on carbonate-rich Marcellus shale core samples: an experimental study. J Petroleum Explor Prod 2021;11(2):725–34.
- [38] You J, Lee KJ. The experimental investigation and data-driven modeling for thermal decomposition kinetics of Green River Shale. Fuel 2022;320:123899.
- [39] Castor SB, Henry CD. Lithium-rich claystone in the McDermitt Caldera, Nevada, USA: Geologic, mineralogical, and geochemical characteristics and possible origin. Minerals 2020;10(1):68.
- [40] Grew ES. The minerals of lithium. Elements: An International Magazine of Mineralogy, Geochemistry, and Petrology 2020;16(4):235–40.

- [41] Sawhney B. Selective sorption and fixation of cations by clay minerals: a review. Clay Clay Miner 1972;20(2):93–100.
- [42] Eberl DD. Alkali cation selectivity and fixation by clay minerals. Clay Clay Miner 1980;28(3):161–72.
- [43] Popova OH, Coleman M, Frye E, Long G, Panarelli E. EIA Marcellus Shale Play Map. American Association of Petroleum Geologists Search and Discovery 2009.
- [44] Zagorski WA, Emery M, Ventura JL. The Marcellus shale play: Its discovery and emergence as a major global hydrocarbon accumulation. 2017.
- [45] Jia Y, Fang Y, Elsworth D, Wu W. Slip velocity dependence of friction-permeability response of shale fractures. Rock Mech Rock Eng 2020;53(5):2109–21.
- [46] Zheng L, Rutqvist J, Birkholzer JT, Liu H-H. On the impact of temperatures up to 200 C in clay repositories with bentonite engineer barrier systems: A study with coupled thermal, hydrological, chemical, and mechanical modeling. Eng Geol 2015;197:278–95.
- [47] Boschetti T. A revision of lithium minerals thermodynamics: Possible implications for fluids geochemistry and geothermometry. Geothermics 2022;98:102286.
- [48] Boschetti T. An update on lithium mica thermodynamics and its geothermometrical application. Geothermics 2023;109:102661.
- [49] Sanjuan B, Gourcerol B, Millot R, Rettenmaier D, Jeandel E, Rombaut A. Lithiumrich geothermal brines in Europe: An up-date about geochemical characteristics and implications for potential Li resources. Geothermics 2022;101:102385.